RM A55K10

RESEARCH MEMORANDUM

INFLUENCE OF THE BODY FLOW FIELD ON THE ZERO-LIFT WAVE DRAG OF WING-BODY COMBINATIONS MODIFIED IN ACCORDANCE WITH THE TRANSONIC AREA RULE

By William A. Page

Ames Aeronautical Laboratory
Moffett Field, Calif.

NATIONAL ADVISORY COMMITTEE
FOR AERONAUTICS
WASHINGTON

February 7, 1956
Declassified October 14, 1957

NATIONAL ADVISORY COMMITTEE FOR AERONAUTICS

RESEARCH MEMORANDUM

INFLUENCE OF THE BODY FLOW FIELD ON THE ZERO-LIFT WAVE DRAG OF WING-BODY COMBINATIONS MODIFIED IN ACCORDANCE WITH THE TRANSONIC AREA RULE

By William A. Page

SUMMARY

An analysis based upon an approximation to the transonic small-disturbance theory is presented which shows an influence of the local Mach number field of the body on the zero-lift wave drag of wing-body combinations modified in accordance with the transonic area rule. The analysis indicates that for a restricted class of indented wing-body combinations the zero-lift wave drag approximates that of the corresponding equivalent body when a Mach number of 1 occurs locally at the wing instead of in the free stream. Comparisons are made between the analysis and available experimental data. The comparisons suggest an explanation for some of the anomalous results obtained by various investigators from tests of indented wing-body combinations.

INTRODUCTION

The transonic area rule as first demonstrated by Whitcomb (ref. 1) has led to the procedure of indenting the bodies of wing-body combinations in the region of the wing in order to reduce the drag rise at sonic speed to the value for the body alone. The results of applying body indentations, as reported by Whitcomb and others, have not been entirely consistent. In some cases a drag rise at sonic speed equal to that of the body alone (the so-called equivalent body of revolution) has been obtained. In other cases the drag rise has been higher than that of the equivalent body.

Some reasons for these inconsistencies have been advanced. Spreiter has shown in reference 2, by an examination of experimental data on the basis of the transonic similarity rules, that if the similarity parameter for aspect ratio and thickness, $A(t/c)^{1/3}$, for a wing becomes too large, the zero-lift drag rise at sonic speed is no longer related by the

transonic area rule to the drag rise of a similar wing of lower aspect ratio and thickness (i.e., lower value of $A(t/c)^{1/3}$). As a result, it can be expected that a similar limit exists on $A(t/c)^{1/3}$ for wings mounted either on indented or unindented bodies above which drag equivalence with the respective equivalent body would not be obtained. Whitcomb also recognized that some limitation should exist since the rule specifies that the wings must be "thin" and of "low aspect ratio." It has also be suggested in reference 3 that flow separation in the region of the body indentation, caused by excessive body surface slopes, would change the effective boundary of the configuration and thereby prevent the attainment of equivalent body drag rise.

In addition to the foregoing two possible sources of a higher drag rise at transonic speeds, an as yet unexplored explanation is offered here, namely, the influence on the drag of the wing of the local Mach number field induced by the body. It was reasoned that the drag of the wing and indentation parts of the configuration would depend primarily upon the value of the local Mach number in the vicinity of the wing instead of the free-stream Mach number. It is the purpose of this paper to investigate the influence on the zero-lift wave drag of indented wing-body combinations of the local Mach number field induced by the body and, by comparisons of the analytical results with experiment, to indicate the extent to which this influence accounts for some of the aforementioned anomalous results of applying the transonic area rule.

SYMBOLS

A	aspect ratio
b	wing span
c	wing-root chord
C_p	pressure coefficient, $\frac{p-p_\infty}{q_\infty}$
$\overline{C_p}$	average value of the pressure coefficient in the region R (defined below)
C_{D_o}'	zero-lift drag coefficient, $\frac{D_o'}{q_\infty S_w}$
C_{D_o}	zero-lift wave-drag coefficient, $\frac{D_o}{q_\infty S_w}$
D_o'	zero-lift drag

D_0 zero-lift wave drag

k $\dfrac{(\gamma+1)M_\infty^2}{U_\infty}$

l body length

M_∞ free-stream Mach number

M_l local Mach number

ΔM $M_l - M_\infty$

$\overline{\Delta M}$ average value of ΔM in the region R (defined below)

q_∞ free-stream dynamic pressure

R small region of the equivalent body flow field corresponding to the region occupied by the wing in the complete configuration flow field

$r(x)$ body radius as a function of x

S_w plan-form area of wing, including part inside body

S_s surface area of configuration

t wing thickness

t_0 wing maximum thickness

U_∞ free-stream velocity

x,y,z longitudinal, lateral, and normal coordinate system with the x axis corresponding to the wind axis

β^2 $M_\infty^2 - 1$

β_1^2 $\beta^2 + k\overline{\varphi_{B_x}}$

γ ratio of specific heats

λ surface slope

φ perturbation potential

φ_x perturbation velocity

$\overline{\varphi_x}$ average value of φ_x in the region R (defined above)

Subscripts

B equivalent body of revolution

C complete configuration, wing-body combination modified in accordance with the transonic area rule

P perturbation shape, the wing and the area-rule body indentation on an infinite cylindrical body

x,y,z derivative with respect to x, y, or z

ANALYSIS

General Method

The basic problem under consideration is to investigate the influence on the zero-lift wave drag of an indented wing-body combination of the local Mach number field induced by the body. To study this problem analytically it is necessary to use the transonic small-disturbance theory, since any simpler theory is incapable of predicting local velocity field effects. The analysis consists of two parts: (1) the determination of an approximate transonic velocity potential about the configuration and (2) the computation of the zero-lift wave drag from knowledge of this velocity potential.

Since the transonic small-disturbance equation is nonlinear, the application of the theory is extremely difficult. Methods for finding solutions for three-dimensional shapes are not available. Accordingly, simplifying assumptions are introduced and only an approximation to the transonic potential is found. For example, this approach is used in references 4 and 5 where the zero-lift wave drag of slender three-dimensional shapes is studied at transonic speeds by use of an approximation based upon slenderness.

Derivation of the Velocity Potential

Consider the wing-body combination modified in accordance with the transonic area rule shown as the complete configuration in sketch (a). The problem is to find an approximation to the transonic potential φ_C about this configuration. Since the transonic area rule states that the drag rise depends primarily upon the longitudinal distribution of area and indicates that a wing-body combination will have a drag rise equal to that of the equivalent body at sonic speed, φ_C, the potential about the complete configuration was related to φ_B, the potential about the equivalent body (the second configuration shown on sketch (a)) by the equation

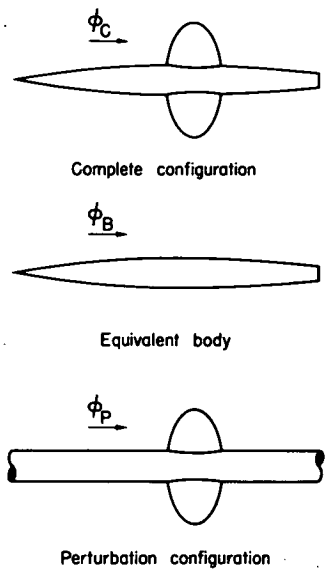

Sketch (a)

$$\varphi_C = \varphi_B + \varphi_P \tag{1}$$

where φ_P can be considered as a difference perturbation potential. The purpose of the remainder of this section will be to show that under certain conditions the perturbation potential, φ_P, can be closely approximated by the linear-theory potential about the third configuration of sketch (a). This perturbation configuration is an area-rule indented wing-body combination resembling the complete configuration, but with an infinite cylindrical body.

The transonic small-disturbance equation expressed in terms of a perturbation potential can be written in the form

$$(\beta^2 + k\varphi_x)\varphi_{xx} = \varphi_{yy} + \varphi_{zz} \; ; \quad k = \frac{(\gamma + 1)M_\infty^2}{U_\infty} \tag{2}$$

where x, y, and z are a longitudinal, lateral, and normal coordinate system with the x axis along the body center line coinciding with the wind axis. For a derivation and discussion of the applicability of this equation see reference 6, pages 327-335. Substituting the value of φ_C from equation (1) in equation (2) gives

$$(\beta^2 + k\varphi_{B_x} + k\varphi_{P_x})(\varphi_{B_{xx}} + \varphi_{P_{xx}}) = \varphi_{B_{yy}} + \varphi_{P_{yy}} + \varphi_{B_{zz}} + \varphi_{P_{zz}} \tag{3}$$

As φ_B by itself is a solution to equation (2), the subtraction of equation (2) from equation (3) yields

$$(\beta^2 + k\varphi_{B_x})\varphi_{P_{xx}} + k\varphi_{P_x}(\varphi_{P_{xx}} + \varphi_{B_{xx}}) = \varphi_{P_{yy}} + \varphi_{P_{zz}} \tag{4}$$

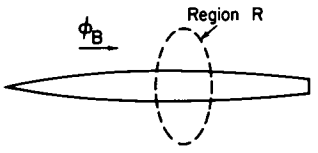

Sketch (b)

A small region, R, of the equivalent body flow field (sketch (b)) is now considered which corresponds to the region about the complete configuration occupied by the wing. In this region the assumption $|\varphi_{B_x} - \overline{\varphi_{B_x}}| \ll |\overline{\varphi_{B_x}}|$ is made regarding the value of φ_{B_x}. The symbol $\overline{\varphi_{B_x}}$ represents the average value of φ_{B_x} in the region R. It is easily recognized that the above relation is equivalent to stating that the local Mach number field about a body of revolution decays slowly in the radial direction at transonic speeds and that over the portion of the body length containing the wing the variation in φ_{B_x} is small. A survey about a representative smooth slender body of revolution, made in the Ames 2- by 2-foot transonic wind tunnel, verified the existence of such a region and indicated that this assumption was reasonable. The results of the survey are presented in Appendix A.

It is further assumed that $|\varphi_{B_{xx}}| \ll |\varphi_{P_{xx}}|$ in the region R. This statement is qualitatively related to the previous assumption, for if φ_{B_x} varies but a small amount, $\varphi_{B_{xx}}$ must be small. Appendix A also presents a comparison between theory and experiment to show that for the test configuration $\varphi_{B_{xx}}$ is small compared with $\varphi_{P_{xx}}$.

With the introduction of these approximations in equation (4), there is obtained for φ_P in the region R

$$(\beta^2 + k\overline{\varphi_{B_x}} + k\varphi_{P_x})\varphi_{P_{xx}} = \varphi_{P_{yy}} + \varphi_{P_{zz}} \tag{5}$$

or

$$(\beta_1^2 + k\varphi_{P_x})\varphi_{P_{xx}} = \varphi_{P_{yy}} + \varphi_{P_{zz}} \tag{6}$$

where

$$\beta_1^2 = \beta^2 + k\overline{\varphi_{B_x}} \tag{7}$$

Since $\beta^2 + k\varphi_x$ equals $M_l^2 - 1$ to the order of accuracy retained in this analysis, the symbol β_1 is recognized as characterizing the average local Mach number of the flow field about the equivalent body in the region of the wing. Moreover, inspection of equation (6) indicates that, in the region R, φ_P satisfies the transonic small-disturbance equation with the free-stream Mach number defined as the average of the local Mach number in R for the equivalent body alone.

In addition to satisfying equation (6) in the region R and equation (4) outside R, φ_P must satisfy conditions determined from the boundary conditions satisfied by φ_C and φ_B. In the region of the wing φ_P must satisfy the same boundary conditions as does φ_C. For a wing-body combination which is symmetrical with respect to the horizontal plane, this condition is given by

$$\left.\frac{\partial \varphi_P}{\partial z}\right|_{z=o} = U_\infty \lambda_C(x,y) \tag{8}$$

where U_∞ is the free-stream velocity and $\lambda_C(x,y)$ is the wing surface slope.

To obtain the boundary condition satisfied by φ_P near the body surface is more complicated. For a circular body, the initial boundary conditions are

$$\left.\frac{\partial \varphi_C}{\partial r}\right|_{r=r_C(x)} = U_\infty \lambda_C(x) \tag{9}$$

and

$$\left.\frac{\partial \varphi_B}{\partial r}\right|_{r=r_B(x)} = U_\infty \lambda_B(x) \tag{10}$$

where $r_C(x)$ and $r_B(x)$ define the body radii of the two configurations. In the region of the body indentation, $r_C(x)$ is not the same as $r_B(x)$. However, for simplicity, it will be assumed here that neither $r_C(x)$ nor $r_B(x)$ differs appreciably from the average value of $r_B(x)$ in this region. Furthermore, since $\lambda_C(x)$ is equal to $\lambda_B(x)$ at other positions on the body outside the indentation, the boundary condition satisfied by φ_P is closely approximated by

$$\left.\frac{\partial \varphi_P}{\partial r}\right|_{r=\bar{r}_B} = U_\infty \lambda_P(x) = U_\infty \left[\lambda_C(x) - \lambda_B(x)\right] \tag{11}$$

where $\bar{r}_B$ is the average body radius in the region of the indentation. This equation indicates that the boundary condition approximately satisfied by φ_P near the body surface is described by an indented infinite cylindrical body. Altogether, equations (8) and (11) indicate that the boundary conditions which apply to φ_P are those of an area-rule indented wing-body combination resembling the complete configuration, but with an infinite cylindrical body rather than a pointed finite body.

At this point in the analysis, it can be said that some progress has been made since the equations and boundary conditions approximately satisfied by φ_P have been determined. However, the problem is still nonlinear, and not presently solvable, since equation (6) is in the form of the transonic small-disturbance equation. It can now be demonstrated that the perturbation potential, φ_P, can be linearized, a step which greatly facilitates the determination of solutions. In reference 7 it is shown that for a configuration described by an equal number of sources and sinks in each plane perpendicular to the wind axis, the velocity potential as calculated by linear theory remains finite as the Mach number approaches and becomes 1. In particular, φ_x remains small compared with U_∞ except, for instance, for singularities at the leading edge of a wing. Similar conditions apply to the perturbation configuration, P, if the approximation of the proportionality of source strength to surface slope is accepted. This approximation is valid for wing-body combinations at or near a Mach number of 1 (see ref. 8).

The preceding arguments have indicated that equation (6) for the perturbation potential, φ_P, can be reduced to linearized form and still produce finite and small values for the perturbation velocities at sonic speed, a result which has an interesting consequence. As the zero-lift wave drag will be zero for this configuration at sonic speed (ref. 7), it can be said that a special class of thickness solutions exists which is valid at this Mach number. These solutions predict the transonic area rule for a configuration that can be described by an equal number of sources and sinks in planes perpendicular to the x axis (i.e., for configurations where the derivative of the area distribution with respect to x is zero everywhere).

Within the framework of the above approximations, the velocity potential at transonic speeds of wing-body combinations modified in accordance with the transonic area rule, for which the local Mach number field about the equivalent body is approximately constant in the corresponding region occupied by the wing, can be determined as follows:

1. The velocity potential about the wing-body combination in the region occupied by the wing is approximated by the sum of two parts; namely, (a) the velocity potential about the equivalent body alone, and (b) the velocity potential about the wing and an infinite cylindrical body having the same indentation volume as the actual body.

2. The velocity potential of the equivalent body is calculated by transonic small-disturbance theory. The velocity potential of the wing and indented infinite cylindrical body is calculated by linear theory, but with the Mach number used in the calculations determined by the average local Mach number of the equivalent body in the corresponding region occupied by the wing.

Calculation of the Zero-Lift Wave Drag

The zero-lift wave drag of the complete configuration is given by

$$D_{0_C} = q_\infty \int_{S_s} \lambda_C C_{p_C} dS_s \tag{12}$$

integrated over the exposed plan-form area of the wing and the surface of the indented body. Using the relationship

$$C_p = -\frac{2\varphi_x}{U_\infty} - \frac{\varphi_y^2 + \varphi_z^2}{U_\infty^2} \tag{13}$$

and equations (1), (11), and (12) gives

$$D_{0_C} = q_\infty \int_{S_s} (\lambda_B + \lambda_P) \left[\left(-\frac{2\varphi_{B_x}}{U_\infty} - \frac{\varphi_{B_y}^2 + \varphi_{B_z}^2}{U_\infty^2} \right) + \left(-\frac{2\varphi_{P_x}}{U_\infty} - \frac{\varphi_{P_y}^2 + \varphi_{P_z}^2}{U_\infty^2} \right) - \frac{2\varphi_{B_y}\varphi_{P_y}}{U_\infty^2} - \frac{2\varphi_{B_z}\varphi_{P_z}}{U_\infty^2} \right] dS_s \tag{14}$$

or

$$D_{0_C} = q_\infty \int_{S_s} \left[\lambda_B C_{p_B} + \lambda_P C_{p_B} + \lambda_B C_{p_P} + \lambda_P C_{p_P} + (\lambda_P + \lambda_B) \left(-\frac{2\varphi_{B_y}\varphi_{P_y}}{U_\infty^2} - \frac{2\varphi_{B_z}\varphi_{P_z}}{U_\infty^2} \right) \right] dS_s \tag{15}$$

An examination of the various terms of equation (15) follows: The first term on the right-hand side of equation (15) represents the drag of the equivalent body; it is the only term "predicted" by the transonic area rule at a free-stream Mach number of 1. The fourth term of equation (15) represents the drag of the wing and area-rule body indentation on an infinite cylinder. It has a value of 0 for a local Mach number of 1. At a free-stream Mach number of 1 its value depends, of course, upon the amount of increase of the local Mach number about the equivalent body and the shape and size of the wing.

The second term represents the action of the equivalent body pressure field on the indented wing-body combination having the infinite cylindrical body. This term can contribute to the drag only within the

region R since λ_P is zero elsewhere. Within this region it has been assumed that the variations in φ_{B_x} are small or, correspondingly, the variations in C_{p_B} are small. The second term can therefore be written as

$$\int_{S_s} \lambda_P C_{p_B} dS_s = \int_R \lambda_P \overline{C_{p_B}} dS_s + \int_R \lambda_P \left(C_{p_B} - \overline{C_{p_B}} \right) dS_s \qquad (16)$$

The first term on the right-hand side of this equation contributes no drag since a constant pressure field acting on the perturbation shape causes no drag force. The second term is small compared with $\int_{S_s} \lambda_B C_{p_B} dS_s$, the term representing the drag of the equivalent body, since λ_P in R is of the order of magnitude of λ_B elsewhere on the body and $C_{p_B} - \overline{C_{p_B}}$ in R is small compared with C_{p_B}.

The third term of equation (15) represents the action of the pressure field of the wing-body combination having the infinite cylindrical body on the equivalent body. Within the region R, this term can be assumed small compared with the term representing the drag of the equivalent body, since C_{p_P} is the same order of magnitude as C_{p_B} and for the smooth slender equivalent bodies considered here λ_B within R would be small compared with λ_P. Evaluation of the possible remaining drag contribution from the third term of equation (15) in the region outside R is difficult to assess because φ_P no longer satisfies a simple equation as it does in R. However, if the linear solution to φ_P is extended along the body surface (one can imagine the region R growing in size, or conversely, the wings becoming smaller), it is found that φ_{P_x} (and also C_{p_P}) rapidly decays toward zero. This is easily seen, for the potential downstream of an equal number of sources and sinks grouped together (i.e., the wing and the area-rule body indentation) resembles more and more closely the potential directly behind a doublet for which $\varphi_x = 0$. In fact, at a local Mach number of 1, φ_{P_x} would be identically zero along the cylindrical body surface. As C_{p_P} outside R can therefore be expected to be small compared with C_{p_B}, the drag contribution from the third term of equation (15) can be expected to be small compared with the drag of the equivalent body.

The last term of equation (15) can be disposed of with reasoning similar to the foregoing when it is noted that, within the region R, φ_{B_y} and φ_{B_z} are small since the body slopes for smooth slender bodies have small values in this region, and outside the region R, the magnitude of φ_{P_y} and φ_{P_z} must be close to zero as can be reasoned from the boundary-condition requirements given by equation (11).

From the foregoing considerations, the total zero-lift wave drag of the complete configuration can be approximated by

$$D_{O_C}(M_\infty) \cong D_{O_B}(M_\infty) + D_{O_P}(M_l) \tag{17}$$

where $D_{O_B}(M_\infty)$ is the zero-lift wave drag of the equivalent body alone and $D_{O_P}(M_l)$ is the zero-lift wave drag of the perturbation configuration (the indented wing-body combination having the infinite cylindrical body). The zero-lift wave drag of the equivalent body, $D_{O_B}(M_\infty)$, must be calculated from the transonic small-disturbance theory at the free-stream Mach number, whereas $D_{O_P}(M_l)$ can be calculated by means of the linear theory but at a Mach number given by the average of the local Mach number field about the equivalent body in the region of the wing. Since D_{O_P} is zero in a sonic flow field and increases as the Mach number is increased, it is clear that equation (17) indicates that the complete configuration can have greater zero-lift wave drag than its equivalent body at a free-stream Mach number of 1. This increase in drag can be attributed to what might be called a Mach number shift effect on the drag of the wing and area-rule indentation parts of the configuration. It must also be remembered that equation (17) has been derived under relatively restrictive conditions; that is, the wing is small relative to the body size and located in a region where the corresponding equivalent body flow field is approximately uniform.

It should be mentioned that as the Mach number is increased somewhat above unity, the transonic analysis presented herein breaks down and linear theory becomes more directly applicable. In that case, equation (17) can be shown to be accurate when both D_{O_B} and D_{O_P} are obtained directly from linear theory at the stream Mach number, if the equivalent body is a so-called minimum drag shape.

COMPARISON OF PREDICTED RESULTS WITH AVAILABLE EXPERIMENTAL DATA

It is the intent of this section to determine whether the theoretical prediction of the previous section is in accord with experiment, and thus to see if the analysis accounts for the anomalous results from tests on indented wing-body combinations. A direct comparison between the predicted value from equation (17) and the experimental value of the zero-lift wave drag of the complete configuration cannot be made since solutions to the transonic small-disturbance equation for bodies of revolution are not available either for the drag, or the local Mach number field about the body. Determination of the usefulness of equation (17) can be made, however, by comparing the predicted value of $C_{D_{O_P}}$ (the zero-lift wave

drag of the wing and indentation parts of the configuration) with the experimental value of $C_{D_{o_P}}$ and obtaining the local Mach number field about the equivalent body either directly from experiment, or from linear-theory calculations.

Experimental values of $C_{D_{o_P}}$, as obtained from available experiments on indented wing-body combinations, will be compared with linear-theory values of $C_{D_{o_P}}$ with and without the correction for the shift in Mach number caused by the velocity field of the body. A description of the means of evaluating the quantities necessary for the comparison between experiment and theory follows:

The linear-theory values for $C_{D_{o_P}}$ were obtained in most cases from the literature; the actual source will be given subsequently on the figures which show the comparisons. The value for the average local Mach number about the equivalent body in the region occupied by the wing was estimated in most cases from experiment, as described in Appendix B. A summary of the results obtained is given in the table of Appendix B. The experimental drag of the wing and indentation parts of the configuration was obtained by subtracting the experimental drag of the equivalent body from the experimental drag of the complete configuration. The zero-lift wave drag of the wing and indentation, $C_{D_{o_P}}$, was estimated in turn by considering it equal to the zero-lift drag rise, which is obtained by subtracting the subsonic drag level from the transonic and supersonic drag values. The quantity subtracted was usually the zero-lift drag at the lowest subsonic Mach number at which data were available. This procedure is equivalent to assuming that the change in friction drag over the Mach number range of interest is negligible and that no serious amount of flow separation takes place.

Figure 1 shows the comparisons between measured characteristics for wing-body combinations modified in accordance with the transonic area rule, and the characteristics estimated by the approximate theory as developed in the preceding section of this report. The upper half of each part of the figure shows the experimental data as obtained from the indicated references. In the lower half of the figure is shown the experimental value of $C_{D_{o_P}}$ as determined from the data in the upper half of the figure. This estimate of zero-lift wave drag of the wing and indentation based upon the experimental data is compared with the linear-theory value of $C_{D_{o_P}}$ and the modified value of $C_{D_{o_P}}$, which is shifted in Mach number (due to the influence of the local Mach number field induced by the body) by the amounts indicated in the table given in Appendix B. Figures 1(a), (e), and (f) definitely show improved agreement between experiment and theory at transonic speeds when the influence of the local Mach number field of

the body is taken into account. Figures 1(b), (c), and (d) represent cases where the influence of the local Mach number field of the body should be negligible, since there was little increase in the local Mach number above the free-stream value at the wing location for the bodies of these examples. Figures 1(b) and (c) show that the experimental value of $C_{D_{o_P}}$ is near zero at a free-stream Mach number of 1, as was expected for these cases. The large increase in the experimental value of $C_{D_{o_P}}$ (e.g., fig. 1(d)) prior to sonic speed is not accounted for by the present theory.

It seems that consideration of the local Mach number field about the equivalent body explains why some indented wing-body combinations exhibit greater zero-lift drag rise at a free-stream Mach number of 1 than the equivalent body. One of the requirements which appears to be necessary for the sonic drag rise to be the same is for the equivalent body to be so shaped as to assure that the local Mach number in the corresponding region occupied by the wing is approximately the free-stream value (as it is for a body with a sufficiently long cylindrical section or for a very slender body).

The preceding analysis or the experimental comparisons shown do not give any direct information regarding the largest aspect ratio and thickness of a wing for which the concept of the transonic area rule can be expected to be valid (ref. 2). The possibility of finding any information on this subject from the present analysis was lost when equation (7) for the perturbation potential, φ_P, was linearized. A systematic series of experimental tests or the appropriate solution to the transonic small-disturbance equation would be necessary for this purpose.

CONCLUDING REMARKS

An approximate transonic analysis, based on relatively restrictive assumptions, has shown that, for indented wing-body combinations for which the wing is small relative to the body size and for which the local Mach number field about the equivalent body is approximately constant in the corresponding region occupied by the wing, the zero-lift wave drag is approximated by the sum of two parts: (1) the zero-lift wave drag of the equivalent body, and (2) the zero-lift wave drag of the wing and an infinite cylindrical body having the same indentation volume as the actual body. The drag of the wing and indented infinite cylindrical body depends on the average local Mach number of the equivalent body in the region occupied by the wing.

Comparisons of the approximate analysis with available experimental data have been made by considering only the zero-lift wave drag of the wing and indentation parts of the configuration. It was shown that agreement between theory and experiment could be improved by taking into consideration the local Mach number field of the equivalent body. This result confirmed the reasoning that the zero-lift drag rise of a wing-body combination modified in accordance with the transonic area rule must exceed that of the equivalent body at a free-stream Mach number of 1 if there is an appreciable increase in the local Mach number field about the equivalent body. The result of the investigation suggests that drag-rise equivalence occurs when a Mach number of 1 occurs locally at the wing instead of in the free stream.

Ames Aeronautical Laboratory
National Advisory Committee for Aeronautics
Moffett Field, Calif., Nov. 10, 1955

APPENDIX A

SURVEY OF THE VELOCITY FIELD ABOUT A BODY OF REVOLUTION AT TRANSONIC SPEEDS

It is the purpose of this section to demonstrate experimentally two features of the flow field about a smooth slender body of revolution at transonic speeds; namely, (1) variations in the local Mach number field are small in the region occupied by a typical wing, and (2) the value of φ_{xx} in this region is small compared to the theoretical value of φ_{xx} for a wing and area-rule body indentation. To obtain this information a survey of the flow about a body of revolution was made in the Ames 2- by 2-foot transonic wind tunnel. The body used was the same as the body of reference 9 and is also the same body as in figure 1(a) of this report. A static-pressure survey was made with a movable, cylindrical axial tube of 1/2-inch diameter extending through the test section parallel to the wind axis of the wind tunnel.

The results of the pressure survey at Mach numbers from 0.98 to 1.10 are shown in figure 2 in the form of contours of the increase in local Mach number over the free-stream value. The contours shown are the difference between the survey about the body of revolution and an empty-tunnel survey. The accuracy of the contours is the order of 0.01 Mach number. Inspection of the figure shows that over the plan form of the elliptical wing (the dashed lines on the figure) the variations in the local Mach number are small. The variations in this region become larger as the Mach number is increased to 1.10.

To determine if the value of φ_{xx} for the body flow field is small compared with values for a typical wing and area-rule indentation, the experimental values (obtained by using $C_p = -(2\varphi_x/U_\infty)$ to relate the pressure coefficient and the velocity potential) are compared in figure 3 with theoretical values for the wing and area-rule body indentation of reference 9 at a Mach number of 1. The figure shows that φ_{xx} for the body alone is negligible compared with the values for the wing and indentation. The theoretical values were determined by simulating the wing with a source-sink sheet (the planar approximation) and the area-rule body indentation by a line of sinks (and sources) along the center line of the body. Under these conditions, where an equal number of sources and sinks exists in every plane normal to the x axis, the two-dimensional equation

$$\varphi_{yy} + \varphi_{zz} = 0 \qquad \text{(A1)}$$

applies (ref. 7). The potential is therefore given by

$$\varphi(y,z;x) = \frac{U_\infty}{2\pi}\left\{\int_{-a(x)}^{a(x)} \lambda(y_1,x)\ln\left[(y - y_1)^2 + z^2\right]dy_1 - \ln(y^2 + z^2)\int_{-a(x)}^{a(x)} \lambda(y_1,x)dy_1\right\} \tag{A2}$$

where $a(x)$ defines the edge of the plan form. For the elliptic plan-form wing with circular-arc section of reference 9 where

$$\frac{t}{c} = \frac{t_o}{c}\left[1 - \frac{x^2}{(c/2)^2} - \frac{y^2}{(b/2)^2}\right] \tag{A3}$$

$\lambda(y_1,x)$ is given by

$$\lambda(y_1,x) = \lambda(x) = -\frac{t_o x}{(c/2)^2} \tag{A4}$$

The second derivative of the potential is found to be

$$\frac{\varphi_{xx}c}{U_\infty} = \frac{\frac{t_o}{c/2}}{\pi}\frac{\frac{xb}{(c/2)^2}}{\sqrt{1-\left(\frac{x}{c/2}\right)^2}}\left\{\frac{3 - 2\left(\frac{x}{c/2}\right)^2}{1-\left(\frac{x}{c/2}\right)^2}\ln\left[\frac{1-\left(\frac{x}{c/2}\right)^2-\left(\frac{y}{b/2}\right)^2}{\left(\frac{y}{b/2}\right)^2}\right] - \frac{2\left(\frac{x}{c/2}\right)^2}{1-\left(\frac{x}{c/2}\right)^2-\left(\frac{y}{c/2}\right)^2}\right\} \tag{A5}$$

APPENDIX B

DETERMINATION OF THE LOCAL MACH NUMBER ABOUT THE EQUIVALENT BODIES OF REVOLUTION OF FIGURE 1

The average local Mach number about the equivalent bodies in the corresponding region occupied by the wing was estimated in most of the examples of figure 1 by reference to experimental pressure distributions. First, the average pressure coefficient in the region occupied by the wing was determined. (The decay of the pressure field of the body over the span of the wing was ignored in those cases in which it was not known.) Second, the average local Mach number in this region was found from the relation

$$C_p = \frac{1}{0.7M_\infty^2}\left[\left(\frac{1 + 0.2M_l^2}{1 + 0.2M_\infty^2}\right)^{-7/2} - 1\right] \tag{B1}$$

In figure 1(a) the average local Mach number was estimated from the pressure survey presented in Appendix A. For figures 1(b), (c), and (d) the average local Mach number was estimated from pressure-distribution measurements on the equivalent body from reference 15. For figures 1(e) and (f) a linear-theory calculation at a Mach number of 1.05, based on the method of reference 16, was used, since an experimental pressure distribution was not available. It was assumed that the pressure distribution so obtained would be representative of values over the Mach number range of 1.00 to 1.10. To show that this was a reasonable assumption, a comparison between linear theory and the experimental pressure distributions for all the bodies (fig. 1) where such data were available is given in figure 4. It is to be noted in part (a) of figure 4 that the pressure distribution was taken off the surface of the body by the indicated amount; whereas the flagged symbols denote measurements on the surface of the body. Here, the linear-theory method of reference 16 tends to overestimate the actual pressure distribution in the region of the wing. The essential feature of figure 4(b) is the collapse of the pressure coefficient back to the free-stream value over the cylindrical portion of the body. Except for the anomalous behavior of the experimental pressure distribution at a Mach number of 1.03 compared with the distributions at Mach numbers of 1.00 and 1.10, the prediction of the theory is fairly accurate. In summary, while the accuracy of the predictions of the linear-theory method of reference 16 in this Mach number range has been shown to be somewhat variable, it can be expected that the theory will serve to give a rough estimate of the pressure distribution on bodies for which no experimental data are available (figs. 1(e) and (f)).

A summarizing table showing the values of the average local Mach number used in the calculation of $C_{D_{o_P}}$ for figure 1 is given below:

Figure 1	Body in figure 4	M_l for $M_\infty = 1.00$	Source
(a)	(a)	1.025	Pressure survey (Appendix A)
(b)	(b)	1.00	Pressure distribution (ref. 15)
(c)	(b)	1.00	Do.
(d)	(b)	1.00	Do.
(e)	(c)	1.04	Linear theory (ref. 16)
(f)	(c)	1.04	Do.

REFERENCES

1. Whitcomb, Richard T.: A Study of the Zero-Lift Drag-Rise Characteristics of Wing-Body Combinations Near the Speed of Sound. NACA RM L52H08, 1952.

2. Spreiter, John R.: On the Range of Applicability of the Transonic Area Rule. NACA RM A54F28, 1954.

3. Whitcomb, Richard T.: Recent Results Pertaining to the Application of the "Area Rule." NACA RM L53I15a, 1953.

4. Harder, Keith C., and Klunker, E. B.: On Slender-Body Theory at Transonic Speeds. NACA RM L54A29a, 1954.

5. Maeder, P. F.: Similarity of Slender-Bodies and Small Aspect Ratio Wing-Body Combinations at Transonic Speeds. TR WT12, Brown University, Division of Engineering, Apr. 1954.

6. Sears, W. R., Editor: General Theory of High Speed Aerodynamics. Vol. VI of High Speed Aerodynamics and Jet Propulsion, Joseph V. Charyk and Martin Summerfield, gen.eds., Princeton University Press, 1954.

7. Heaslet, Max. A., Lomax, Harvard, and Spreiter, John R.: Linearized Compressible-Flow Theory for Sonic Flight Speeds. NACA Rep. 956, 1950. (Supersedes NACA TN 1824)

8. Lomax, Harvard: The Wave Drag of Arbitrary Configurations in Linearized Flow as Determined by Areas and Forces in Oblique Planes. NACA RM A55A18, 1955.

9. Baldwin, Barrett S., and Dickey, Robert R.: Application of Wing-Body Theory to Drag Reduction at Low Supersonic Speeds. NACA RM A54J19, 1955.

10. Jones, Robert T.: Theory of Wing-Body Drag at Supersonic Speeds. NACA RM A53H18a, 1953.

11. Hoffman, Sherwood: An Investigation of the Transonic Area Rule by Flight Tests of a Sweptback Wing on a Cylindrical Body With and Without Body Indentation Between Mach Numbers 0.9 and 1.8. NACA RM L53J20a, 1953.

12. Holdaway, George H.: Comparison of Theoretical and Experimental Zero-Lift Drag-Rise Characteristics of Wing-Body-Tail Combinations Near the Speed of Sound. NACA RM A53H17, 1953.

13. Kelly, Thomas C.: Transonic Wind-Tunnel Investigation of the Effects of Body Indentation for Boattail and Cylindrical Afterbody Shapes on the Aerodynamic Characteristics of an Unswept-Wing-Body Combination. NACA RM L54A08, 1954.

14. Morgan, Francis G., Jr., and Carmel, Melvin M.: Transonic Wind-Tunnel Investigation of the Effects of Taper Ratio, Body Indentation, Fixed Transition, and Afterbody Shape on the Aerodynamic Characteristics of a 45° Sweptback Wing-Body Combination. NACA RM L54A15, 1954.

15. Robinson, Harold L.: Pressures and Associated Aerodynamic and Load Characteristics for Two Bodies of Revolution at Transonic Speeds. NACA RM L53L28a, 1954.

16. Thompson, Jim Rogers: A Rapid Graphical Method for Computing the Pressure Distribution at Supersonic Speeds on a Slender Arbitrary Body of Revolution. NACA TN 1768, 1949.

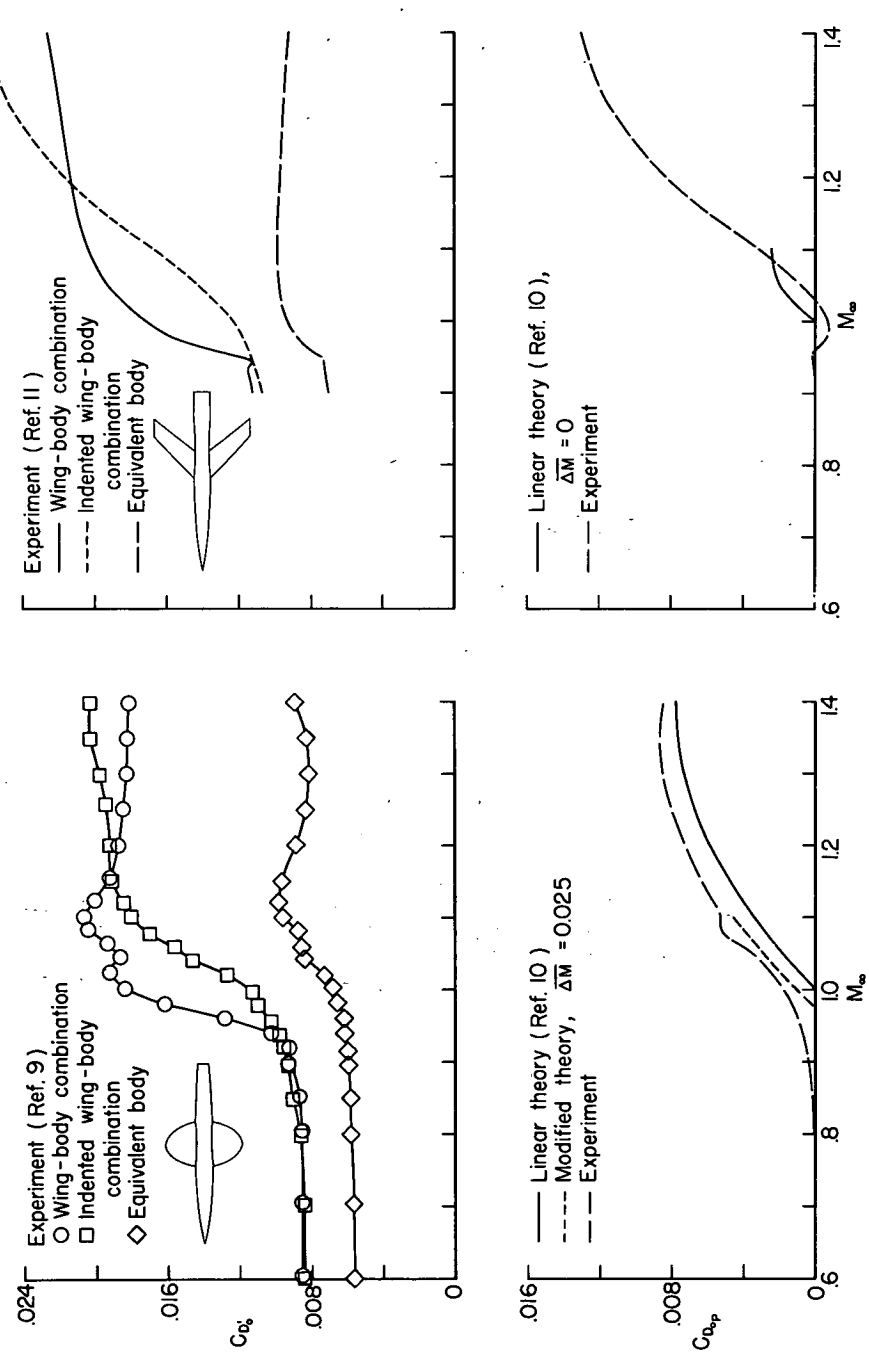

(a) Wing-body configuration of reference 9.

(b) Wing-body configuration of reference 11.

Figure 1.- Basic data and a comparison between experiment and theory for the zero-lift wave drag of the wing and area-rule body indentation.

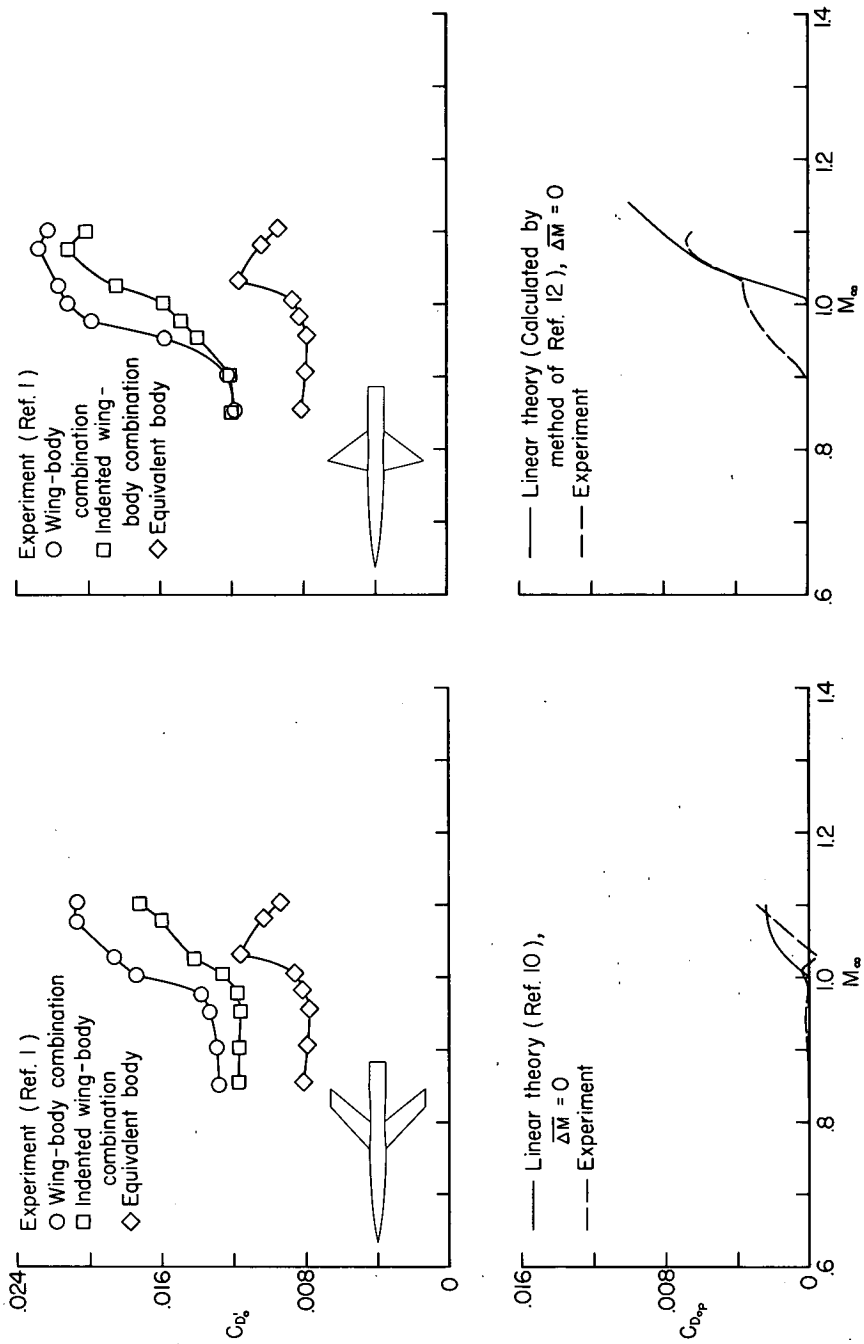

(c) Swept-wing-body configuration of reference 1.

(d) Unswept-wing-body configuration of reference 1.

Figure 1.- Continued.

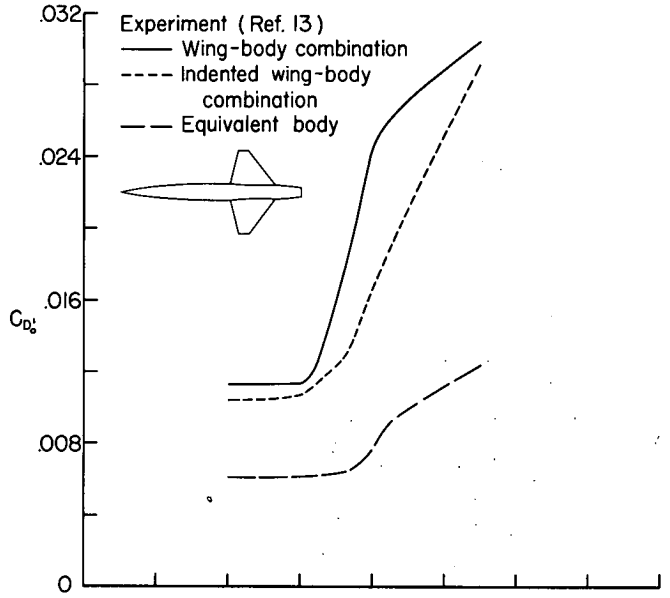

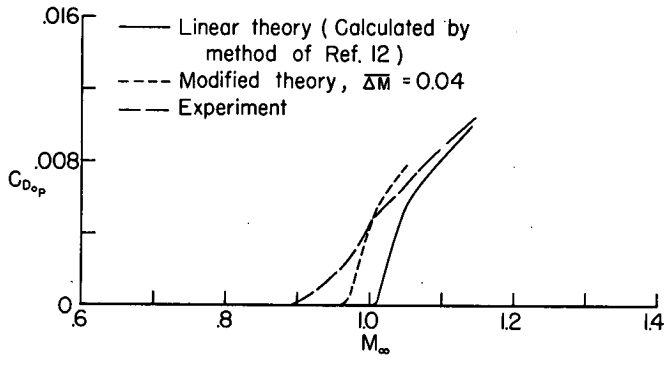

(e) Wing-body configuration of reference 13.

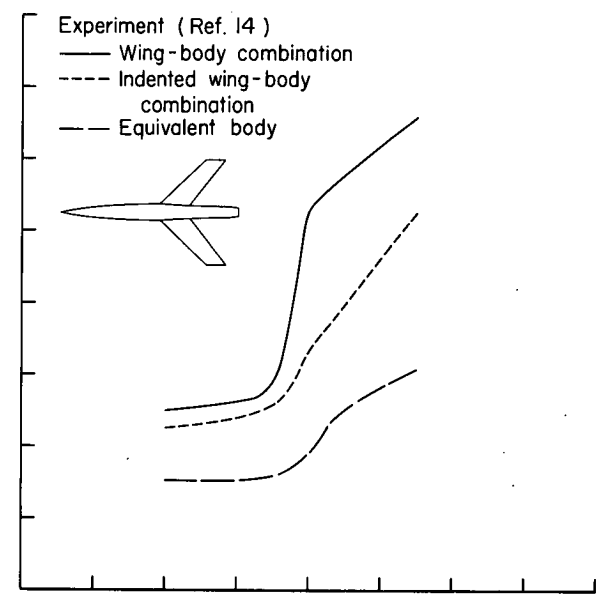

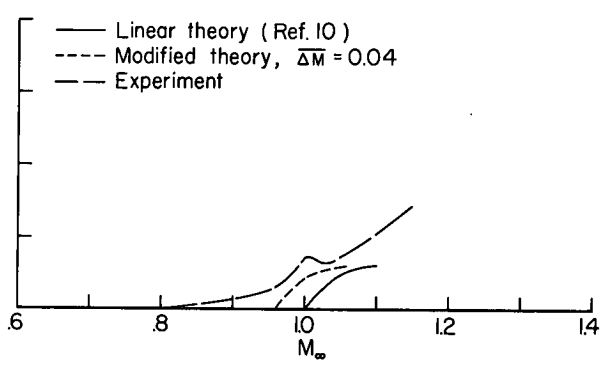

(f) Wing-body configuration of reference 14.

Figure 1.- Concluded.

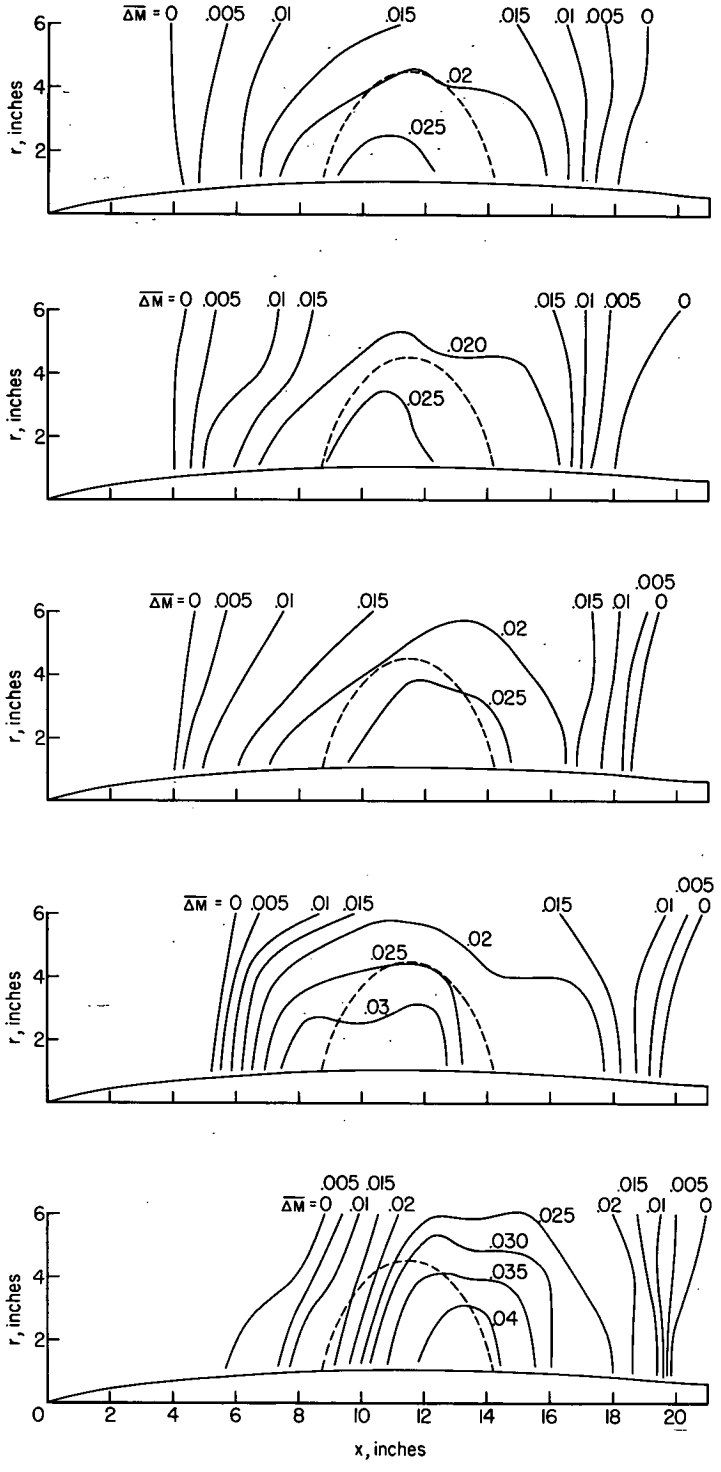

Figure 2.- Experimental local Mach number distribution about a Sears-Haack-Karman ogive body of revolution at transonic Mach numbers.

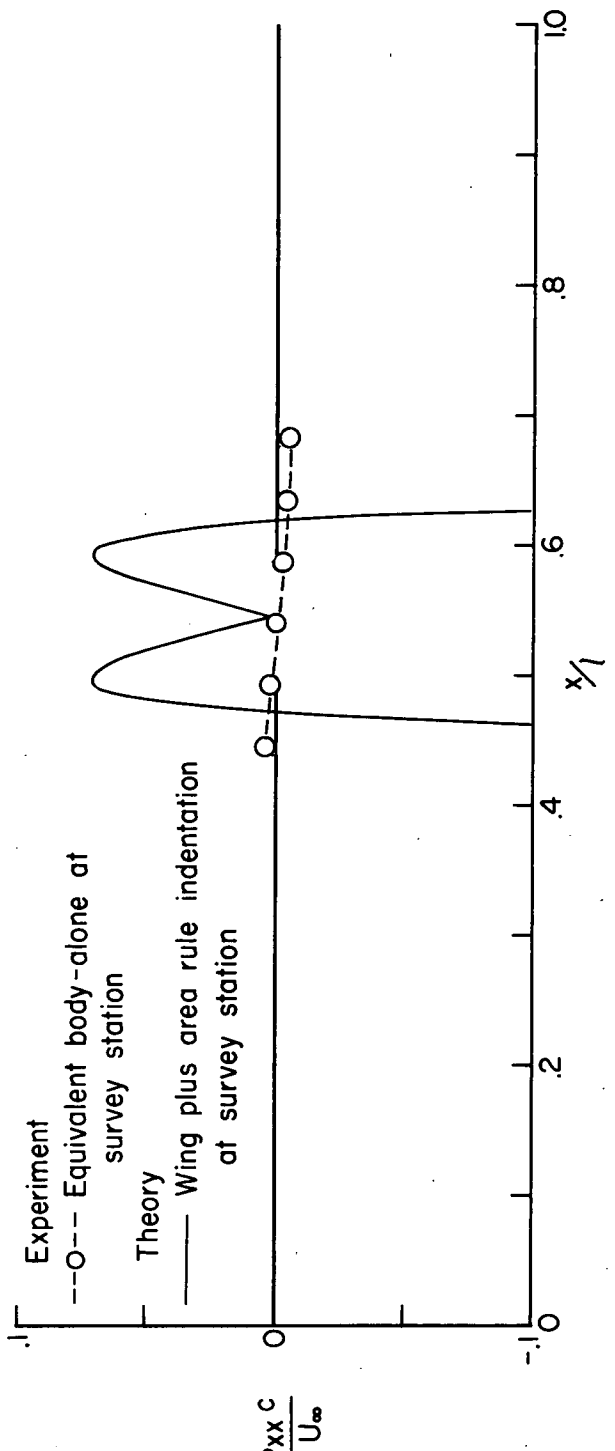

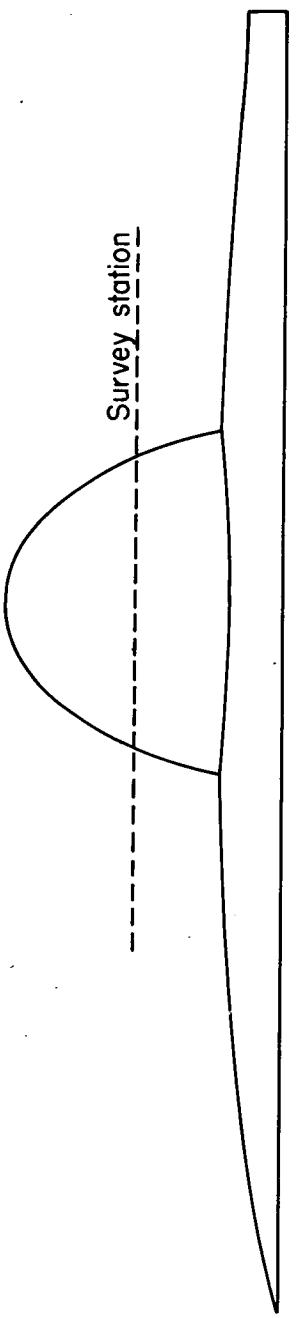

Figure 3.- Experimental body alone Φ_{Bxx} and theoretical Φ_{Pxx} for an elliptic wing and area rule body indentation at $M_\infty = 1.0$.

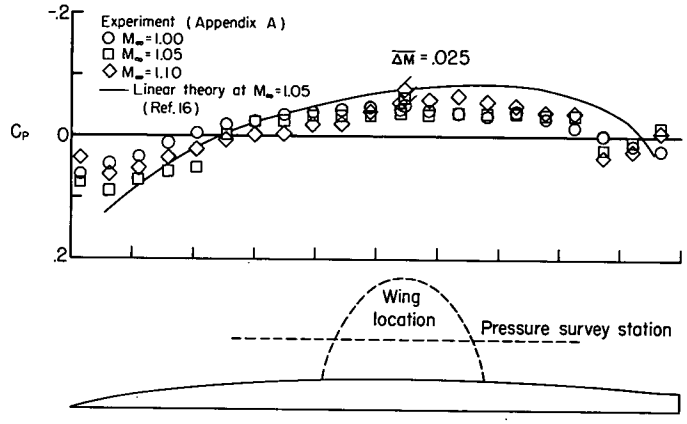

(a) Equivalent body of figure 1(a).

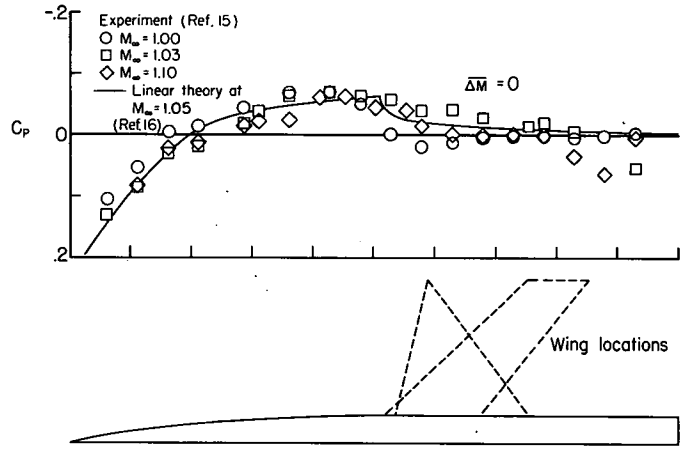

(b) Equivalent body of figure 1(b), (c), and (d).

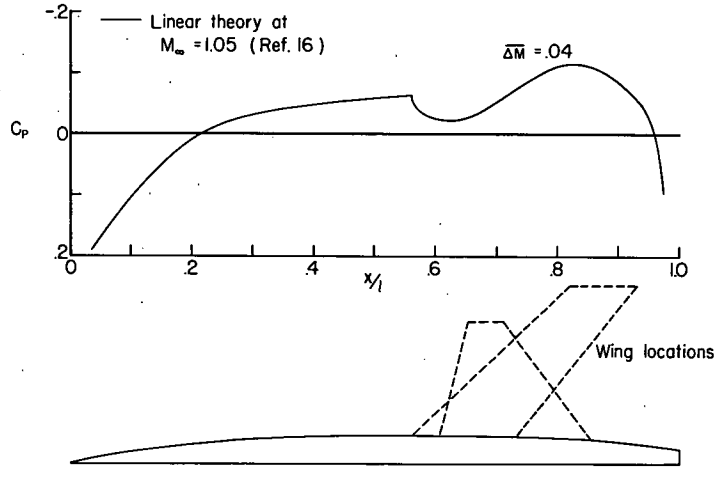

(c) Equivalent body of figure 1(e) and (f).

Figure 4.- Experimental and theoretical pressure distributions about the equivalent bodies at transonic Mach numbers.